ARTICLE IN PRESS

ELSEVIER

Materials Characterization 5514 (2002) xxx–xxx

MATERIALS CHARACTERIZATION

Quantification of the evolution of the 3D intermetallic structure in a 6005A aluminium alloy during a homogenisation treatment

N.C.W. Kuijpers [a,*], J. Tirel[b], D.N. Hanlon[a], S. van der Zwaag[a,b]

[a]*Netherlands Institute for Metals Research, Rotterdamseweg 137, 2628 AL Delft, The Netherlands*
[b]*Laboratory for Materials Science, Delft University of Technology, Rotterdamseweg 137, 2628 AL Delft, The Netherlands*

Received 25 July 2002; accepted 8 August 2002

Abstract

In the case of aluminium alloys, a postcasting homogenisation heat treatment is applied in order to improve extrudability. During this homogenisation, a phase transformation occurs and the intermetallic structure evolves from an interconnected network of plate like structures into a more discrete distribution of particles. The morphology of these intermetallics has been the subject of many studies employing conventional 2D characterization. However, recently, it has been shown that 2D analyses can be misleading and that techniques suitable for quantification of 3D structures can provide more reliable information. In this study, serial sectioning and 3D reconstruction techniques were used to reveal the three-dimensional morphology, connectivity and distribution of the intermetallic microstructure, and the evolution of these parameters during homogenisation. The qualitative and quantitative analysis of the reconstructed intermetallic microstructures, with particular reference to the determination of the spatial distribution of the absolute, mean and Gaussian curvature is discussed.

Keywords: Aluminium alloys; 3D morphology; Serial sectioning; Homogenisation; Intermetallics; Curvature distribution; Phase transformation

1. Introduction

In the case of commercial Al extrusion alloys, a homogenisation heat treatment of the as-cast material is required to improve ductility to such a degree as to enable efficient extrusion [1]. The optimisation of such extrusion processes will depend on a thorough understanding of the reactions occurring during homogenisation and, in particular, the morphological evolution of the intermetallics during the homogenisation process.

The principle processes which occur during this homogenisation are a phase transformation from monoclinic β-Al_5FeSi to cubic α_c-$Al_{12}(FeMn)_3Si$ and a gradual morphological change from interconnected plate structures to more discrete, cylindrical structures [2–4]. The morphology of these intermetallics has been the subject of many studies employing conventional 2D characterization. Such two dimensional metallographic techniques are usually used to provide information regarding morphology, connectivity or distribution of the intermetallic microstructure. However, it has recently been shown that such 2D

* Corresponding author. Tel.: +31-15-278-2268; fax: +31-15-278-6730.
E-mail address: N.C.W.Kuijpers@tnw.tudelft.nl (N.C.W. Kuijpers).

1044-5803/02/$ – see front matter © 2002 Published By Elsevier Science Inc.
PII: S1044-5803(02)00289-9

analyses [5,6] can be misleading and that techniques for a proper quantification of 3D structures need to be employed. The focus of this work has therefore been placed on obtaining detailed 3D information regarding the evolution of the microstructure morphology during homogenisation heat treatment.

2. Experimental techniques

2.1. Alloy composition and heat treatment

The alloy under investigation is an industrial DC-cast 6005A aluminium alloy. The chemical composition for this alloy is shown in Table 1. Material was received in the form of an as-cast billet with a diameter of 254 mm. To ensure the same starting as-cast microstructure for each sample, all metallographic samples were sectioned from locations approximately 25 mm from the edge of the billet.

For the 3D reconstructions presented in this report, six conditions at different stages of homogenisation were produced and two different homogenisation temperatures were used. Table 2 shows the homogenisation conditions and fraction transformed from β-Al_5FeSi to α_c-$Al_{12}(FeMn)_3Si$ as determined using Scanning Electron Microscopy and Electron Dispersive X-ray analysis for the samples under investigation [7].

2.2. Sample preparation, serial sectioning and 3D image reconstruction

A sample of each condition under investigation was metallographically prepared in the usual manner to a 1/4 μm colloidal silica polished finish. Each sample was then etched in 0.5% HF solution for 4 s in order to enhance the contrast between the intermetallics and the aluminum matrix.

For the 3D reconstruction, a rectangular region of interest was chosen on each metallographic section and was labelled using Vickers microhardness indentations. The size of the area of interest was in each case 200 μm in both the *x*- and *y*-directions. Micrographs of the regions of interest were then taken using a Leica TCS SP laser scanning confocal microscope (LSCM) equipped with a digital image capture facility. The confocal microscope was preferred for this application over conventional instruments since, in addition to affording a significant extension of resolution, imaging at a discrete wavelength was found to provide sharp contrast without the need for heavy etching in HF [8]. Samples were then lightly repolished using 1/4 μm colloidal silica in order to remove a thin surface layer. Microhardness indentations were then used to relocate the area of interest and photomicrographs of the region were again taken. This process was subsequently repeated approximately 40 times to create a vertical stack of serial 2D sections at regular intervals along the *z*-axis. The LSCM software enabled a topographical analysis of each of the sections to be conducted in order to check parallelism and to correct for tilt between sections. This also enabled the depth of material removed between sections to be established since the remaining depth of the hardness indents could be accurately measured. The total depth sectioned in this manner was approximately 40 μm in the *z*-direction for each sample. The serial sections were then used for 3D reconstruction of the intermetallics. The 3D reconstruction of the intermetallics was created using a medical tomography software package (surfdriver), which processes the 2D serial sections.

Table 1
The chemical composition (wt.%) of the 6005A Al alloy under investigation

Al	Si	Mg	Fe	Mn	Zn	Other
Balanced	0.83	0.70	0.27	0.18	0.02	≤ 0.01

Table 2
Conditions and fraction transformed from β-Al_5FeSi to α_c-$Al_{12}(FeMn)_3Si$ for the investigated samples

Homogenisation time (min)	0	30	480	60	1920	1920
Temperature of homogenisation (°C)	none	540	540	590	540	590
Fraction transformed from β-Al_5FeSi to α_c-$Al_{12}(FeMn)_3Si$ (%)	5	20	50	80	80	100

2.3. Numerical method for the local, Gaussian and the mean curvature

The surface curvature is an important factor in the transformation, since it provides an indication of local variations in surface energy. The local curvature at one point corresponds to the reciprocal of the radius of a sphere which best conforms to the surface at this point.

A 3D surface has two principal curvatures. They are defined as the minimum and the maximum of the curvatures of the intersection between a plane containing the normal and the surface and are called k_1 and k_2, respectively. The principal curvatures are equal to the eigenvalues of the determinant of the differential of the normal to the surface. The absolute curvature (A) is defined by the maximal absolute principal curvature. The Gaussian curvature is the product of the two principal curvatures:

$$K = k_1 k_2 \tag{1}$$

The mean curvature, as the name suggests, is the mean value of the curvature over all possible directions:

$$H = \frac{1}{2}(k_1 + k_2) \tag{2}$$

The Gaussian (K) and mean curvature (H) are coupled according to the following equations [9]:

$$\frac{\partial H}{\partial T} = -(2H^2 - K)v - \frac{1}{2}\left(\frac{\partial^2 v}{\partial^2 x_1} + \frac{\partial^2 v}{\partial^2 x_2}\right) \tag{3}$$

$$\frac{\partial K}{\partial T} = -2HKv - H\left(\frac{\partial^2 v}{\partial^2 x_1} + \frac{\partial^2 v}{\partial^2 x_2}\right) + \sqrt{H^2 - K}\left(\frac{\partial^2 v}{\partial^2 x_1} - \frac{\partial^2 v}{\partial^2 x_2}\right) \tag{4}$$

where T is the time, v the velocity of the surface along the surface normal and x_1, x_2 represent the two principal directions along the surface. The coupling of the mean and Gaussian curvatures implies that the signs of both Gaussian and mean curvatures describe the morphology of the intermetallic microstructure. Together, the Gaussian and mean curvatures provide an essential measure of the morphology since they enable a saddle-shaped, a convex and concave surfaces to be distinguished. The sign of the Gaussian and mean curvature enables a qualitative classification of morphological character. Table 3 shows that the morphologies can fall into six basic classes: convex, concave, flat, peak, pit and saddle morphologies [10]. When the Gaussian curvature for a given discrete location (point) on the surface under analysis is negative, the form of the surface is approximately hyperbolic, and the local surface is saddle-like (i.e. the point is bounded by regions exhibiting both convex and concave curvatures). When the Gaussian curvature is zero, the surface surrounding the point is only cylindrical if the mean curvature is nonzero. If,

Table 3
Surface interpretation of Gaussian curvature (K) and the mean curvature (H)

Sign	K<0	K=0	K>0
H<0	**Concave saddle** In one orthogonal axis the slope increases rapidly (concave) whilst in the other the slope slightly falls away. 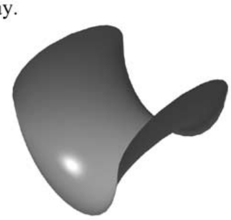	**Trough** Negative shape of cylinder: In one orthogonal direction there is an increase of slope (concave) whilst in the other there is no slope. 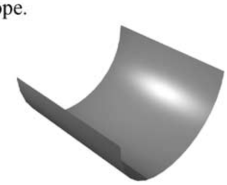	**pit** Negative of spheroid shape. Form is concave. The slope increases in all directions. 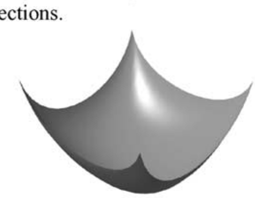
H=0	**symmetric saddle** 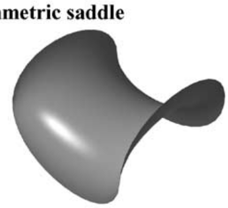	**flat surface** 	-
H>0	**convex saddle** In one orthogonal axis the slope falls away rapidly (convex) whilst in the other direction the slope slightly increases. 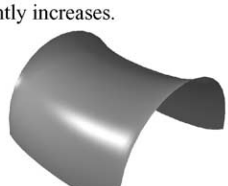	**convex cylindrical** Cylindrical shape. In one orthogonal direction the slope falls away (convex) and in the other orthogonal direction there is no slope. 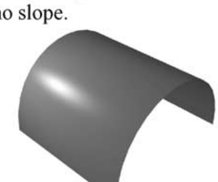	**spheroid** Form is convex. The slope falls away in all directions. 

The intermetallic surface is in all cases the upper surface depicted in the diagrams.

on the other hand, the mean curvature is zero, then the surrounding surface is planar.

3. Results

3.1. 3D qualitative observations

3D reconstructions of the intermetallic microstructure were produced from the 2D cross-sections. Example 2D images taken from a stack, used for such a 3D reconstruction, are shown in Fig. 1. Two

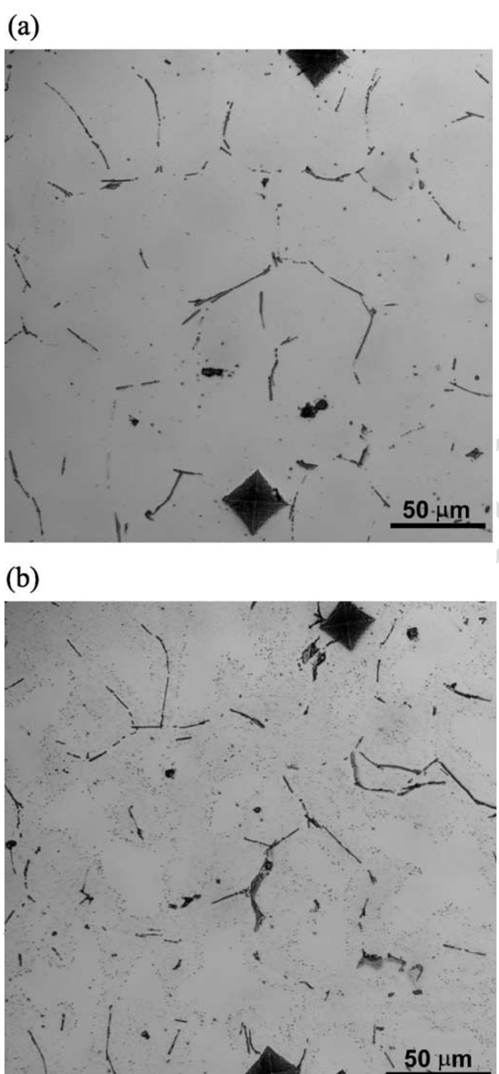

Fig. 1. Two examples of 2D serial sections used for 3D reconstruction. (a) $z = 1$ µm, (b) $z = 30$ µm. The photomicrographs show the microstructure after 30 min homogenisation at 540 °C. The Vickers microhardness indentations, used for alignment of the micrographs, are also visible.

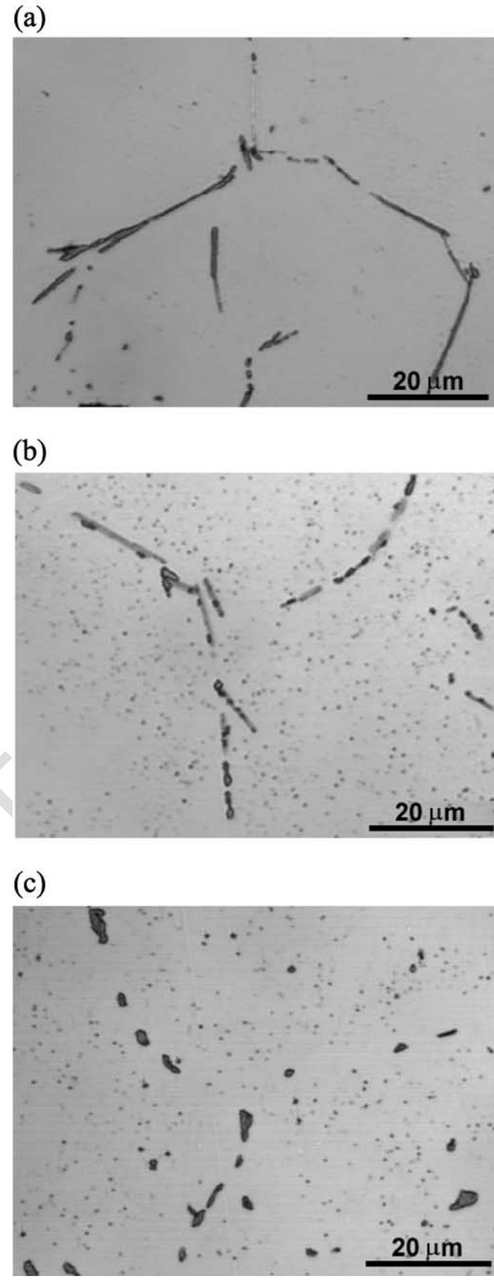

Fig. 2. Photomicrographs showing the intermetallic structure (a) lightly homogenised for 30 min, (b) partially homogenised for 480 min and (c) heavily homogenised for 1920 min at 540 °C.

of the indents, used to adjust alignment and to measure the thickness of materials removed, are visible in these figures.

Fig. 2 shows an overview of the conventional 2D micrographs produced for the three extreme states: lightly homogenised, partially homogenised and

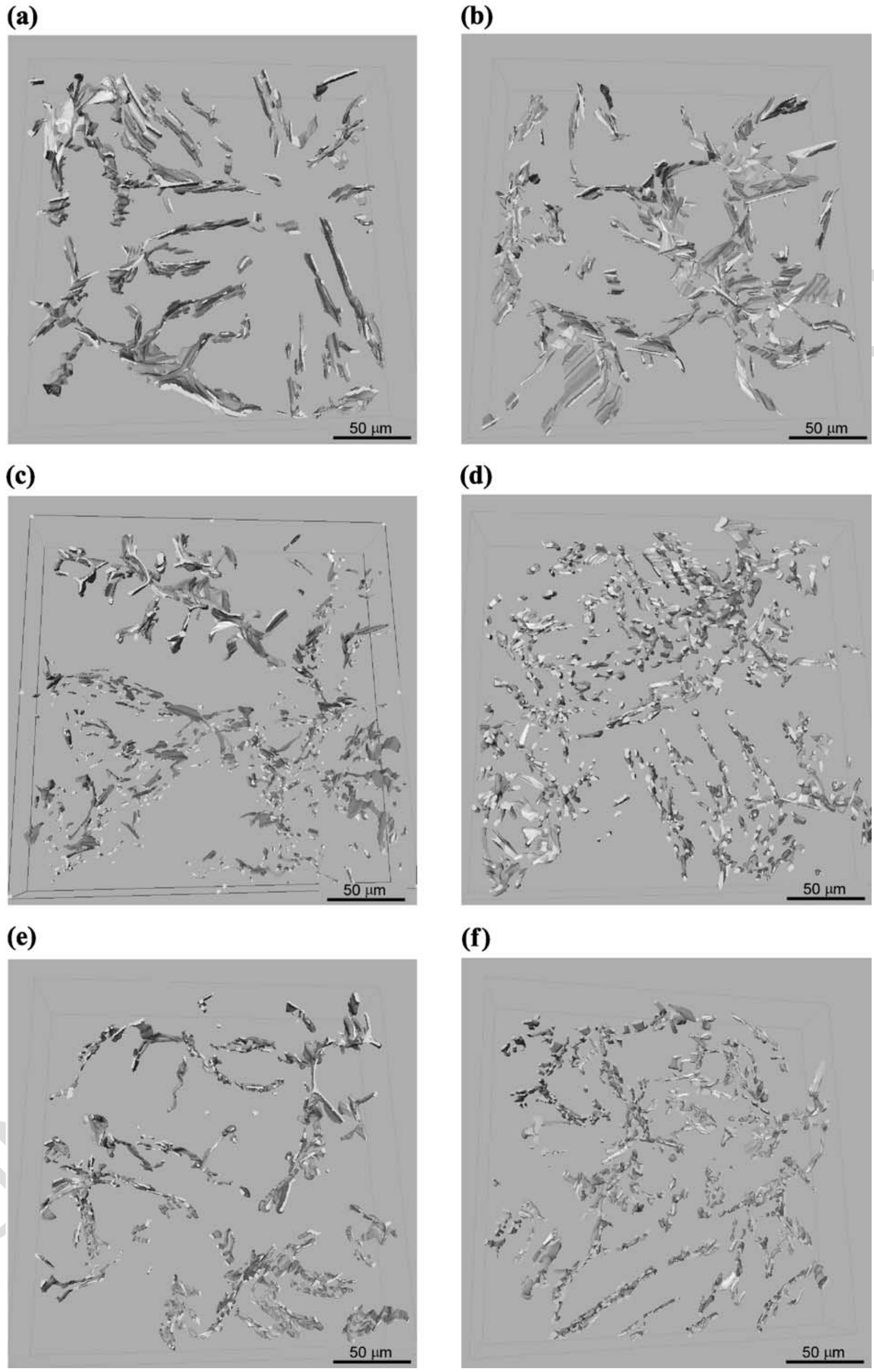

Fig. 3. Surface-rendered 3D reconstructions of aluminium alloy intermetallic microstructure after heat treatment. (a) As-cast, (b) 30 min homogenised at 540 °C, (c) 480 min homogenised at 540 °C, (d) 1920 min homogenised at 540 °C, (e) 60 min homogenised at 590 °C, (f) 1920 min homogenised at 590 °C. The indicated boxes have a dimension of $200 \times 200 \times 40$ μm for all pictures.

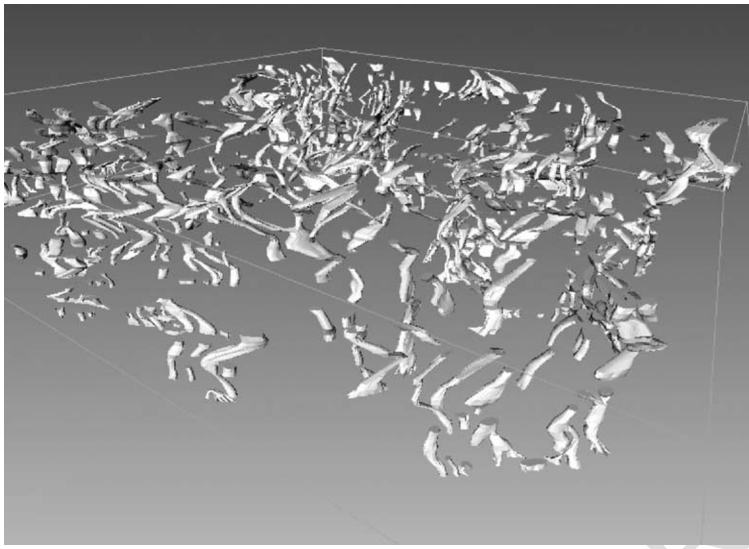

Fig. 4. Cylindrical-shaped α-particles in the surface-rendered 3D reconstruction of aluminium alloy intermetallic microstructure after heat treatment for 1920 min homogenised at 590 °C. The indicated box has a dimension of $200 \times 200 \times 40$ μm.

heavily homogenised. For the partially transformed sample, the etching produced contrast between the β-Al_5FeSi phase, which appears light grey, and the α_c-$Al_{12}(FeMn)_3Si$ phase, which appears dark grey.

The 3D reconstructions of the intermetallic for the six conditions studied are shown in Fig. 3. These images reveal that the coarse planar interconnected β-Al_5FeSi intermetallics break up into more discrete α_c-$Al_{12}(FeMn)_3Si$ particles. The 3D image in Fig. 4 shows that the morphology of the intermetallics in the heavily homogenised structure is cylindrical rather than spherical.

Furthermore, the 3D analysis provides detailed information regarding the spatial distribution of the intermetallics. The interconnectivity of the intermetallics is high when the β-Al_5FeSi phase is the dominant phase and this connectivity decreases as the transformation β-Al_5FeSi to α_c-$Al_{12}(FeMn)_3Si$ proceeds. However, the particle distribution remains inhomogeneous even at long homogenisation times with α particles remaining distributed in stringers along the length of the prior β network.

3.2. Area-to-volume ratio analysis

Table 4 shows the volume-to-surface ratio obtained from the 3D reconstructions by image analysis. The very small intermetallic particles, which are close to the limit of the resolution of the technique (<0.5 μm), are not measured in the 3D reconstruction, therefore the intermetallic volume fraction measured from the 3D reconstructions is lower than the total volume fraction, as measured from 2D micrographs. From the 3D observation, it can be conducted that the morphology for the as-cast sample and the sample homogenised for 30 min at 540 °C is plate like. The surface-to-volume ratio can be calculated from the following equations:

$$\frac{V}{S} = \frac{l\omega\delta}{2(\omega l + l\delta + \omega\delta)} \tag{6}$$

Where l is the length of the plate, ω the width and δ the thickness. If we assume that the thickness

Table 4
Quantitative values as calculated from the 3D reconstruction

Homogenisation time (min)	0	30	480 (α-phase)	480 (β-phase)	60	1920	1920
Temperature of homogenisation (°C)	none	540	540	540	590	540	590
Fraction transformed from β-Al_5FeSi to α_c-$Al_{12}(FeMn)_3Si$ (%)	5	20	50	50	80	80	100
Volume/surface (μm)	0.23	0.20	0.04	0.11	0.21	0.25	0.22

is negligible compared to the length and the width, we obtain:

$$\frac{V}{S} = \frac{\delta}{2} \tag{7}$$

From this equation and the volume-to-surface ratio, an average thickness of the plate can be calculated. For the as-cast and 30 min homogenised at 540 °C conditions, this yields thicknesses equal to 0.46 and 0.40 μm, respectively.

Based on the 3D observations, the intermetallics observed in samples homogenised for 1920 min at 540 °C, 60 min and 1920 min at 590 °C, respectively, appear to have a cylindrical morphology. As previ-

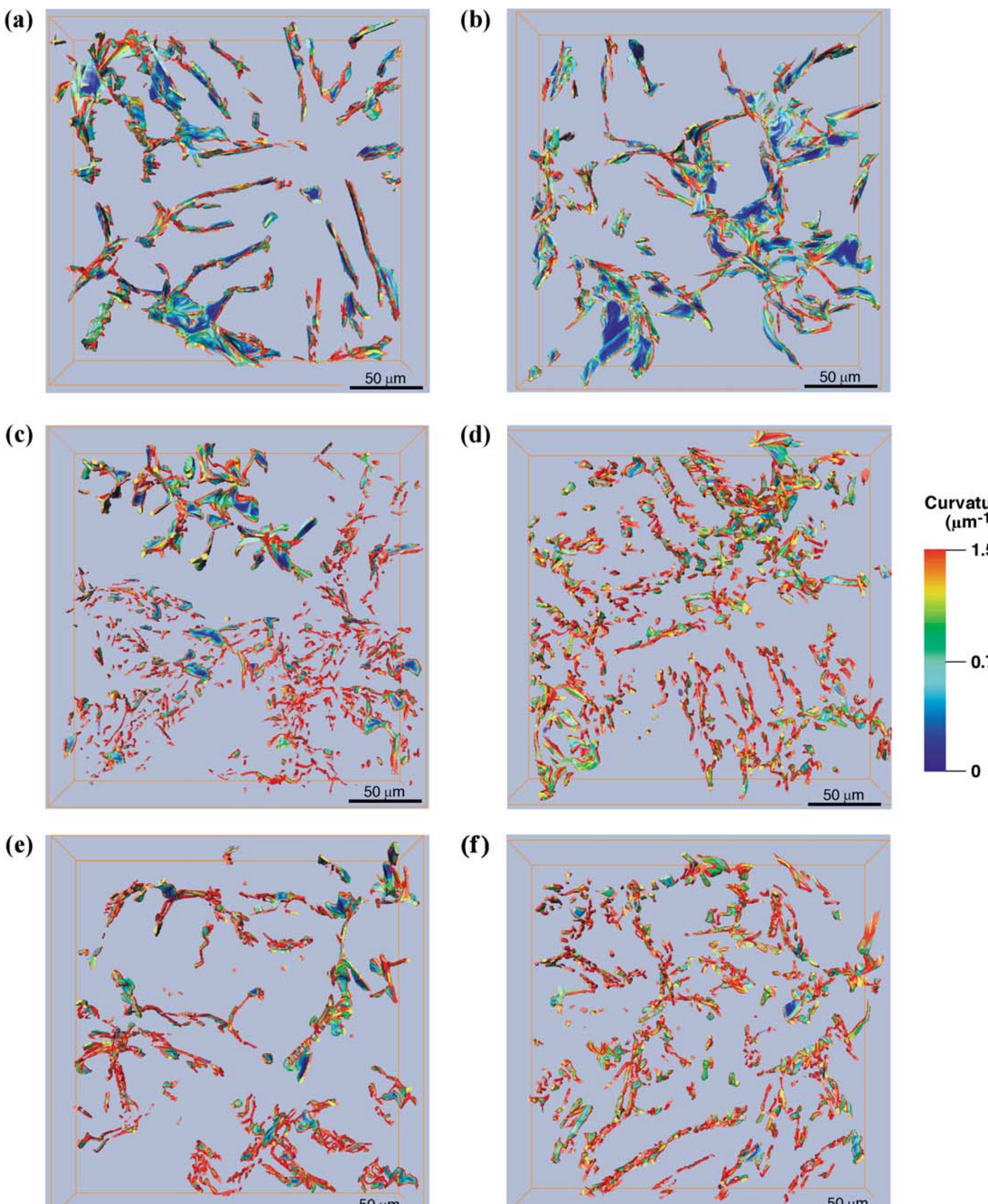

Fig. 5. Colour-coded images showing curvatures for the structures shown in Fig. 4. (a) As-cast, (b) 30 min homogenised at 540 °C, (c) 480 min homogenised at 540 °C, (d) 1920 min homogenised at 540 °C, (e) 60 min homogenised at 590 °C, (f) 1920 min homogenised at 590 °C. The indicated boxes have a dimension of 200 × 200 × 40 μm for all pictures.

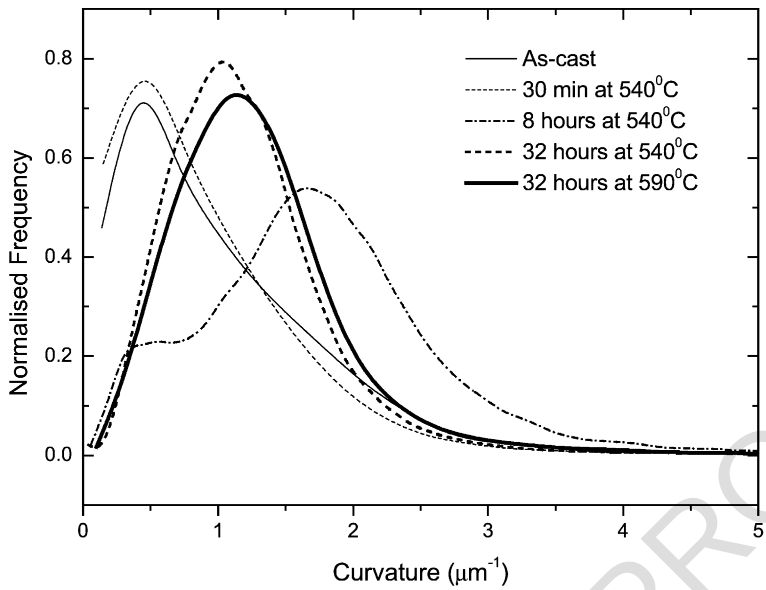

Fig. 6. Frequency plot of the absolute curvature for the complete homogenised series.

ously, the volume and surface fraction can be calculated from:

$$\frac{V}{S} = \frac{\pi R^2 l}{2\pi R l} = \frac{R}{2} \qquad (8)$$

where l is the length of the cylinder and R the radius. Using this equation and the volume-to-surface ratio measured, the average radius of the cylinder was calculated to be 0.50, 0.44 and 0.42 μm for the three samples, respectively.

The 2D analysis on the same samples gives radii of 0.70, 0.67 and 0.74 μm. 2D measurements are consistent with sectioning errors which may be expected to yield a larger value of R.

3.3. Quantification using local curvature

Fig. 5 shows the 3D reconstructions of the structures of Fig. 3 after quantification of the local curvature. The variations in local curvature are denoted by a colour scale.

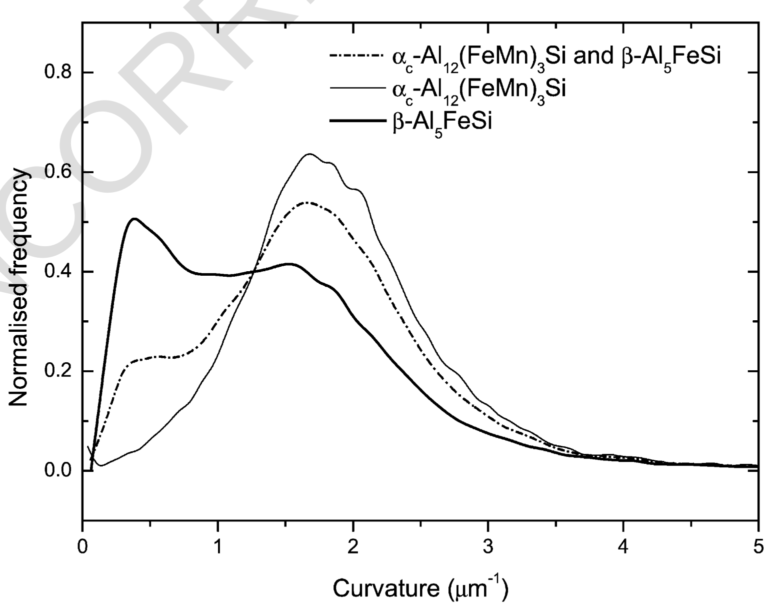

Fig. 7. Frequency plot of the absolute curvature for the sample partially homogenised for 480 min at 540 °C.

These figures clearly show a change of the intermetallic curvature distribution during the homogenisation process. The blue colour corresponds to a flat surface (low curvature), whereas the red colour indicates a round surface (high curvature).

Fig. 6 compares the frequency distribution of absolute curvatures as determined for five samples. This figure shows, with the exception of the sample homogenised for 480 min at 540 °C, that the density of high curvature increases and the density of low curvature decreases at longer homogenisation times. The peak shift to the right and change in distribution (less skewed) indicates an increased curvature and a new curvature distribution. Also, the maximum of the curvature of the intermetallics, which occurs in the lightly homogenised state, is not equal to zero but equal to approximately 0.4 μm^{-1}. This implies that on average the β plates are not truly flat, but show local curvature fluctuations, as would be expected. The curvature distribution of the two first states, as-cast and 30 min homogenised at 540 °C, is equivalent, which indicates that only a limited morphological change occurs during the early stage of transformation from β-Al_5FeSi to α_c-$Al_{12}(FeMn)_3Si$. At intermediate homogenisation times, which yield partial transformation, a more complex distribution, showing two maxima, is obtained. This can be explained by a contribution from the curvatures of both α_c-$Al_{12}(FeMn)_3Si$ and β-Al_5FeSi phases in a binomial distribution.

Fig. 7 shows the absolute curvatures for the β-Al_5FeSi phase, the α_c-$Al_{12}(FeMn)_3Si$ phase, and the addition of curvatures of β-Al_5FeSi and α_c-$Al_{12}(FeMn)_3Si$, in a sample homogenised for 480 min at 540 °C.

The distribution of the curvature for the β-Al_5FeSi phase presents two peaks centered on 0.4 and 1.6 μm^{-1}, respectively. The first peak indicates a low curvature, which corresponds to the mean value found previously for the absolute curvature of the as-cast and 30 min homogenised at 540 °C samples. The second peak indicates a high mean curvature, which is characteristic for a cylindrical or spherical morphology. Therefore, the first peak of the β-Al_5FeSi particles in a partially transformed sample corresponds to the β-Al_5FeSi intermetallics, which remain untransformed. The second peak corresponds to the β-Al_5FeSi plates, which have broken up to form more cylindrical shape during the phase transformation of β-Al_5FeSi to α_c-$Al_{12}(FeMn)_3Si$.

The distribution of the absolute curvature for the α_c-$Al_{12}(FeMn)_3Si$ phase reveals one single peak centered on approximately 1.6 μm^{-1}, which is characteristic of a spherical or cylindrical shape. This curvature is higher than the curvatures observed for the complete transformed α particles (see Fig. 6). Probably, the initial small sizes of the α_c-$Al_{12}(FeMn)_3Si$ phase yield a higher curvature of the α particles.

Fig. 8 provides a comparison of the absolute curvature distributions for two samples with the same fraction transformed but obtained for different homogenisation conditions: one sample has been homogenised for 60 min at 590 °C, whereas the other has been homogenised for 1920 min at 540 °C. The distribution of the absolute curvature for these samples is slightly different. The maximum peak of the absolute curvature

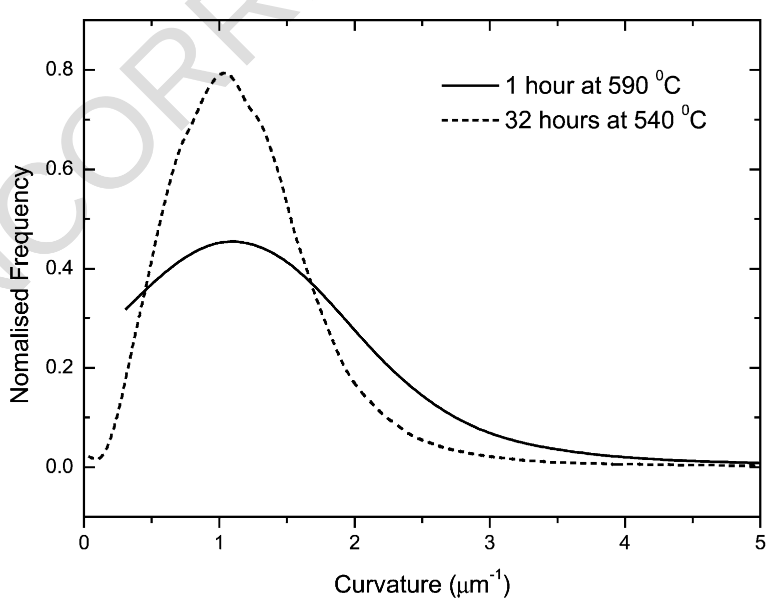

Fig. 8. Frequency plot of the absolute curvature for the sample homogenised for 60 min at 590 °C and 1920 min at 540 °C.

is centered, in both cases, on approximately 1 μm^{-1}. However, the sample homogenised for 60 min at the higher temperature of 590 °C exhibits a shift in the distribution to higher absolute curvatures than the sample homogenised for 1920 min at 540 °C.

3.4. Quantification using Gaussian and mean curvature

Fig. 9a and b shows the distribution of the Gaussian and the mean curvatures for the homogenised series investigated.

From these graphs and based on the surface interpretation of the Gaussian and the mean curvature (Table 3), the pattern of morphological evolution of the intermetallic phases can be determined in greater detail. The distribution of the Gaussian curvature (Fig. 9a) is centered on approximately zero for all the samples investigated which implies that the average morphology for the intermetallics is planar if the mean curvature is also equal to zero or cylindrical if it is not. The distribution of the mean curvature (Fig. 9b) changes with the degree of homogenisation and the homogenisation temper-

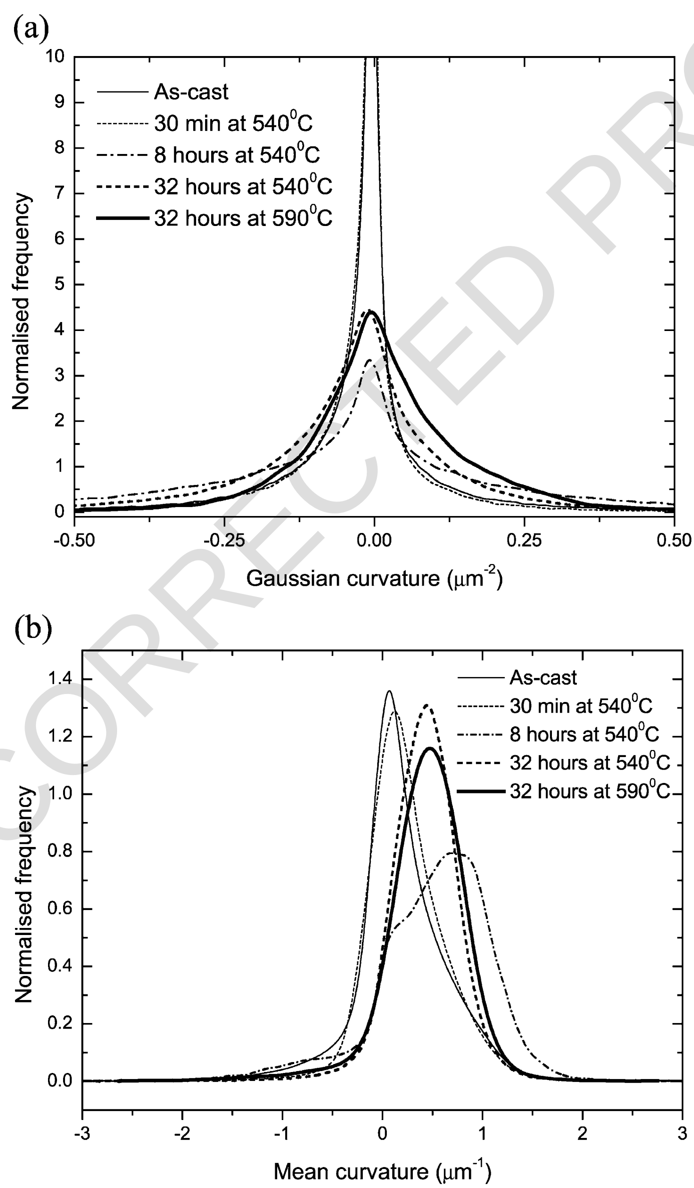

Fig. 9. Frequency plot of (a) the Gaussian curvature, (b) the mean curvature for the complete homogenised series.

Table 5
Surface interpretation of the homogenised series according to the sign of the Gaussian and mean curvature

Sample	Mode of Gaussian curvature (K, μm^{-2})	Mode of mean curvature (H, μm^{-1})	Morphology according to the signs of K and H
As-cast	0.0 (strong peak)	0.0	strongly plate-like
30 min at 540 °C	0.0 (strong peak)	0.0	strongly plate-like
480 min at 540 °C	0.0 (low peak)	1.0 (low intensity)	cylindrical-like with a widespread distribution of radius
1920 min at 540 °C	0.0	0.5	cylindrical
1920 min at 590 °C	0.0	0.5	cylindrical

ature. The as-cast sample and the sample lightly homogenised for 30 min at 540 °C have a symmetrical mean curvature distribution centered on zero, which suggests an elongated surface which is slightly rippled, as was expected from the plate-like morphology of the β-Al_5FeSi. The distribution is

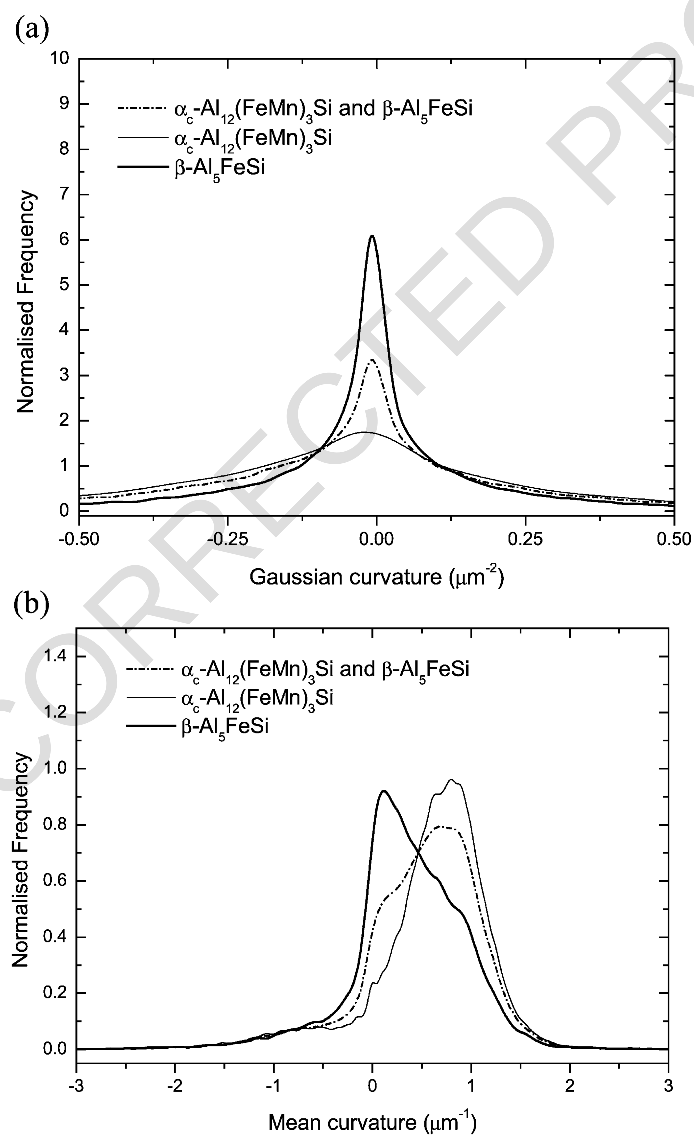

Fig. 10. Frequency plot of (a) the Gaussian curvature, (b) the mean curvature for the sample homogenised for 480 min at 540 °C.

Table 6
Surface interpretation of the Gaussian and the mean curvature signs for the sample partially homogenised for 480 min at 540 °C

	Mode of Gaussian curvature (K, μm^{-2})	Mode of mean curvature (H, μm^{-1})	Morphology according to the signs of K and H
β-Al_5FeSi phase	0.0 (strong peak)	0.0	plate-like
α_c-$Al_{12}(FeMn)_3Si$ phase	0.0 (low peak)	1.0	cylindrical-like

biased towards the positive scale for the samples heavily homogenised (1920 min at 590 and 540 °C) and partially homogenised (480 min at 540 °C), which implies on average a convex surface. These observations indicate that a major morphological change of the intermetallics occurs during the homogenisation for a range of homogenisation time between 30 and 480 min at 540 °C.

Table 5 shows an evaluation of the intermetallic morphology for the samples homogenised for different conditions according to the sign of the Gaussian and the mean curvature.

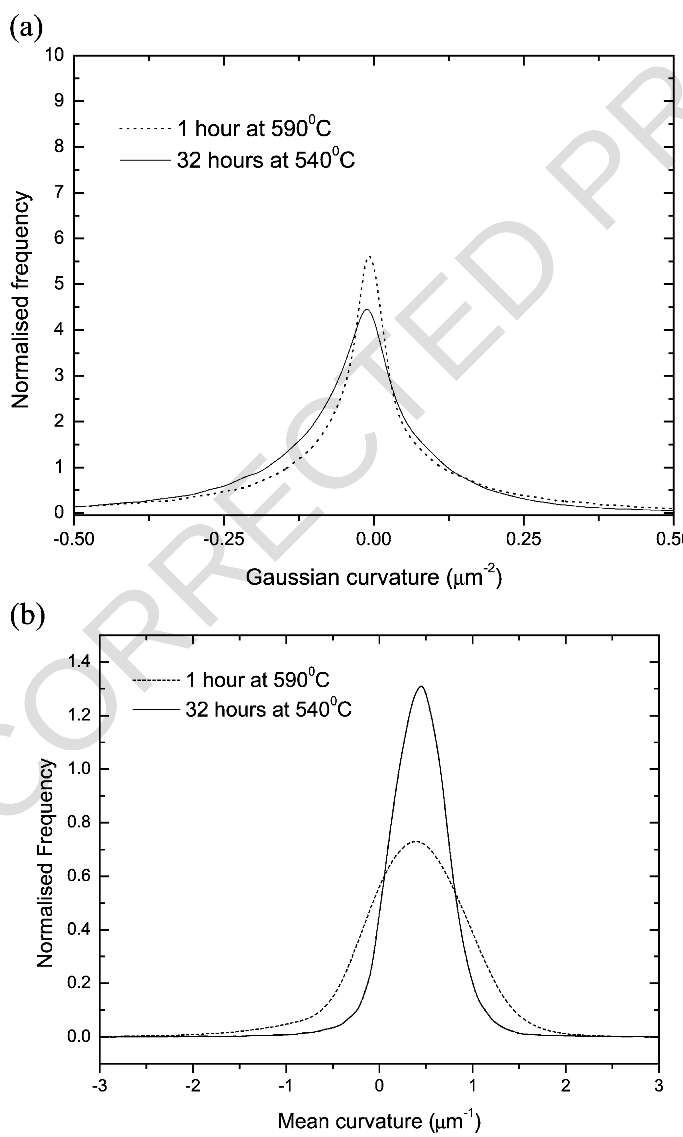

Fig. 11. Frequency plot of (a) the Gaussian curvature, (b) the mean curvature for the samples homogenised for 60 min at 590 °C and 1920 min at 540 °C.

Table 7

Sample	Gaussian curvature with highest appearance (K, μm^{-2})	Mean curvature with highest appearance (H, μm^{-1})	Morphology according to the signs of K and H
Homogenised for 60 min at 590 °C	0.0	0.5 (strong peak)	cylindrical-like with widespread radius distribution
Homogenised for 1920 min at 540 °C	0.0	0.5 (low peak)	cylindrical-like with narrow radius distribution

Fig. 10a and b shows the distribution of the Gaussian and the mean curvature for the sample partially homogenised for 480 min at 540 °C. The contributions of phases β-Al_5FeSi and α_c-$Al_{12}(FeMn)_3Si$ have been separated and analysed separately. The maximum in the distribution of the mean curvature for the β-Al_5FeSi phase is centered on zero, whereas the distribution for the α_c-$Al_{12}(FeMn)_3Si$ phase is biased toward the positive and is centered on $0.75 \mu m^{-1}$. These observations allow us to conclude that the morphology of the β-Al_5FeSi phase in this state is still plate-like, whereas the morphology of the α_c-$Al_{12}(FeMn)_3Si$ phase appears to be convex due to the growth of the α_c-$Al_{12}(FeMn)_3Si$ nuclei.

Table 6 shows an evaluation of the intermetallic morphology for the sample partially homogenised for 480 min at 540 °C according to the sign of the Gaussian and the mean curvature. The average morphology corresponding to the α_c-$Al_{12}(FeMn)_3Si$ phase is cylindrical-like, whereas for the β-Al_5FeSi phase, the morphology is strongly plate-like.

Fig. 11a and b shows the mean and the Gaussian curvature for the samples heavily homogenised for 60 min at 590 °C and 1920 min at 540 °C, respectively. These samples correspond to two different homogenisation conditions that lead to the same fraction transformed, 80%.

Table 7 represents the interpretation of the morphology according to the Gaussian and the mean curvatures signs for these two samples. The sample homogenised at 540 and 590 °C both have a cylindrical morphology, however, at 590 °C the intermetallics have a narrower radius distribution.

4. Discussion

If the different observations, quantifications and calculations are linked together, the morphological evaluation of the intermetallic microstructure for each homogenised state can be made with a relatively high degree of accuracy. The phase transformation from β-Al_5FeSi to α_c-$Al_{12}(FeMn)_3Si$ phase, which occurs during the heat treatment, plays an essential role in the overall morphological change of the microstructure. The morphological evolution of the intermetallics during the homogenisation heat treatment gives some indication of the stages occurring during the transformation process. Such data are crucial as input data for transformation models and model validation.

The results show that for homogenisation at 540 °C, the transformation occurs in a few stages, indicated by (A), (B) and (C):

(A) In as-cast samples, plate-like intermetallics are present and, in the early stages of transformation (up to 20%), the plate-like shape of the intermetallics is still pronounced. The calculation of the area-to-volume ratio gives valuable information regarding the morphologies in the lightly and heavily homogenised states. The thickness of the plates for the as-cast and 30 min homogenised at 540 °C conditions is approximately the same (0.46 and 0.40 μm), which indicates that the β-plates break up only at the edges during the β-Al_5FeSi to α_c-$Al_{12}(FeMn)_3Si$ phase transformation. The plate-like morphology of the β-Al_5FeSi plates for the partially transformed sample is in line with previously recorded LSCM observations on deep etched samples which showed plate-like β-Al_5FeSi intermetallics with rounded nuclei of α on the edges and on the faces [11].

(B) At an intermediate transformation stage (50%), the small α nuclei start to grow on top of the β-Al_5FeSi plates. Observations showed that these α particles have a mode absolute curvature of 1.6 μm^{-1}, corresponding to diameters of 0.6 μm. The results in Fig. 10 showed that those α_c-$Al_{12}(FeMn)_3Si$ phases are already cylindrical at this stage of transformation, however, the weak peak in the Gaussian curvature distribution in Fig. 10a reveals that this remains a wide range of morphologies.

(C) Late in the transformation the α_c-$Al_{12}(FeMn)_3Si$ particles become clearly cylindrical and the connectivity decreases. The mode of absolute curvature of the α particles decreases to 1 μm^{-1}, thus, the radius of the particles increases. For the heavily homogenised (80% transformed) and fully homogenised samples, it can be seen that the diameter of the cylinders are comparable which indicates that the morphology of the intermetallics does not change for the range of 75–100% transformed.

The effect of the temperature on the homogenisation was shown in Fig. 11 for two samples with the same fraction transformed. Although the peak positions of the frequencies of mean curvature are approximately the same for both temperatures, the radius distribution is narrower for the lower T (540 °C). This is also clearly visible in 3D (Fig. 11), showing that the structure at 540 °C is finer and less connected than at 590 °C. While this is an observation based on limited data, it nevertheless implies that homogenisation temperature has an influence on the morphological evolution during heat treatment.

5. Conclusions

The 3D characterization technique by serial sectioning reveals qualitative and quantitative data regarding the morphology of the metallic microstructure which would be impossible to obtain by 2D analysis.

The morphology of the intermetallics at the early stages of the transformation β-Al_5FeSi to α_c-$Al_{12}(FeMn)_3Si$ is predominantly plate-like and interconnected. Nucleation of the α_c-$Al_{12}(FeMn)_3Si$ phase occurs on the initial β-Al_5FeSi plates. In the first half of the transformation, these nuclei grow and the β-Al_5FeSi plates break up at their edges; Leading to both growth of the α_c-$Al_{12}(FeMn)_3Si$ and morphological evolution of the β-Al_5FeSi, the morphology changes mainly in the first half of the transformation.

In the second half of the transformation, the initial α_c-$Al_{12}(FeMn)_3Si$ nucleus becomes more cylindrical and the connectivity decreases dramatically. Nevertheless, the morphology is stabilised to a cylindrical morphology for the α_c-$Al_{12}(FeMn)_3Si$ particle. The spatial distribution of the α_c-$Al_{12}(FeMn)_3Si$ cylinders still closely reflects the spatial distribution of the original β-Al_5FeSi plates.

Acknowledgements

This research was carried out under project number MP 97009-3 in the framework of the strategic research program of the Netherlands Institute for Metals Research in the Netherlands (www.nimr.nl).

References

[1] Zajac S, Hutchingson B, Johanssons A, Gullman LO. Microstructure control and extrudability of Al–Mg–Si Alloys microalloyed with manganese. Mater Sci Technol 1994;10:323–33.
[2] Tanihata H, Sugawara T, Matsuda K, Ikeno S. Effect of casting and homogenizing treatment conditions on the formation of Al–Fe–Si intermetallic compounds in 6063 Al–Mg–Si alloys. Mater Sci 1999;34:1205–10.
[3] Griger A, Stefaniay V. Equilibrium and non-equilibrium intermetallic phases in Al–Fe and Al–Fe–Si alloys. Mater Sci 1996;31:6645–52.
[4] Onurlu S, Tekin A. Effect of heat-treatment on the insoluble intermetallic phases present in an AA-6063 alloy. Mater Sci 1994;29:1652–5.
[5] Alkemper J, Voorhees PW. Three-dimensional characterization of dendritic microstructures. Acta Mater 2001;49:897–902.
[6] Kral MV, Spanos G. Three-dimensional analysis of proeutectoid cementite precipitates. Acta Mater 1999; 47(2):711–24.
[7] Kuijpers NCW, Kool WH, Koenis PTG, Nilsen KE, Todd I, van der Zwaag S. Assessment of different techniques for quantification of intermetallics in AA 6xxx alloys. Mater Charact [submitted for publication].
[8] Hanlon DN, Todd I, Rainforth WM, van der Zwaag S. The application of laser scanning confocal microscopy to tribological research. Wear, 2001 [in press].
[9] Drew DA. Evolution of geometric statistics. J Appl Math 1990;50(3):649–53.
[10] Yarger RWI, Queck FKH. Surface parameterization in volumetric images for feature classification. IEEE International Symposium of Bio-Informatics and Bio-Engineering, BIBE 2000, Washington, DC, 2000. p. 297–303.
[11] Kuijpers NCW, Tirel J, Hanlon DN, van der Zwaag S. On the characterisation of the α_c-$Al_{12}(FeMn)_3Si$ nuclei on β-Al_5FeSi intermetallics by Laser Scanning Confocal Microscopy. Alum Trans, 2001 [in press].